Detection of the kinematic Sunyaev-Zel'dovich (kSZ) effect with DESI galaxy clusters and Planck in Fourier-space

Reporter: Shaohong Li
Supervisor: Yi Zheng, Kwan Chuen Chan

School of Physics and Astronomy,
SUN YAT-SEN University

October 27, 2023

Contents

Background

What is the kSZ effect (Sunyaev and Zeldovich, 1980)

kSZ

kSZ effect: The secondary anisotropy of the CMB temperature caused by the scattering off of CMB photons by free electrons with bulk motions

The kSZ effect directly detects the momentum of the free electrons in the universe. It helps us constrain the Dark Energy, Modified Gravity models and the universal baryon distribution.

$$\begin{aligned}\delta T_{\rm kSZ}(\hat{\boldsymbol{n}}) &= -T_{\rm CMB}\sigma_T \int d\ell \frac{\boldsymbol{v}_e(\boldsymbol{x})\cdot\hat{\boldsymbol{n}}}{c} n_e(\boldsymbol{x}) \\ &= -\bar{\tau} T_{\rm CMB}\boldsymbol{v}_e(\boldsymbol{x})\cdot\hat{\boldsymbol{n}}\end{aligned} \tag{1}$$

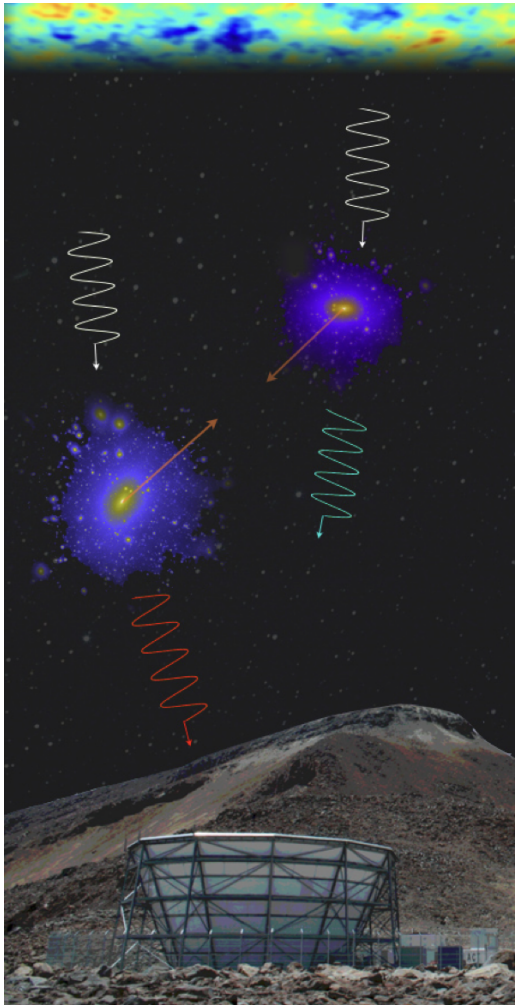

Main interest

Interest

- The kSZ signal produced by baryons in dark matter halos;
- The distribution of baryons in dark matter halos is studied by kSZ signals.

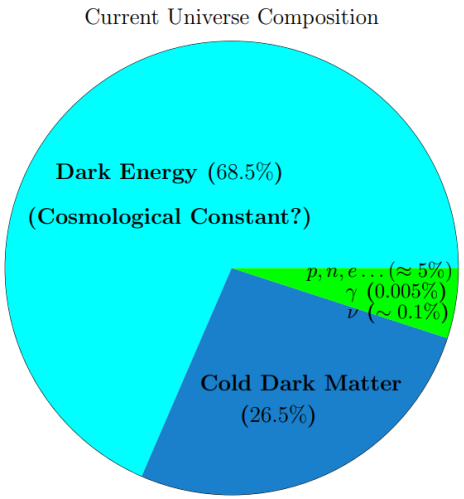

Figure: Universe composition in standard cosmological model.

baryon

- The term baryon represents normal matter formed from odd quark antiquark combinations, overwhelmingly protons and neutrons. Hence baryons make up the nucleons of the periodic table and all that that entails, including us, the Earth and the stars.

Data

The Planck CMB map (http://www.esa.int/Planck) and The Data Release 9 of DESI Legacy Imaging survey (Yang et al., 2021) (Yang et al., 2022)

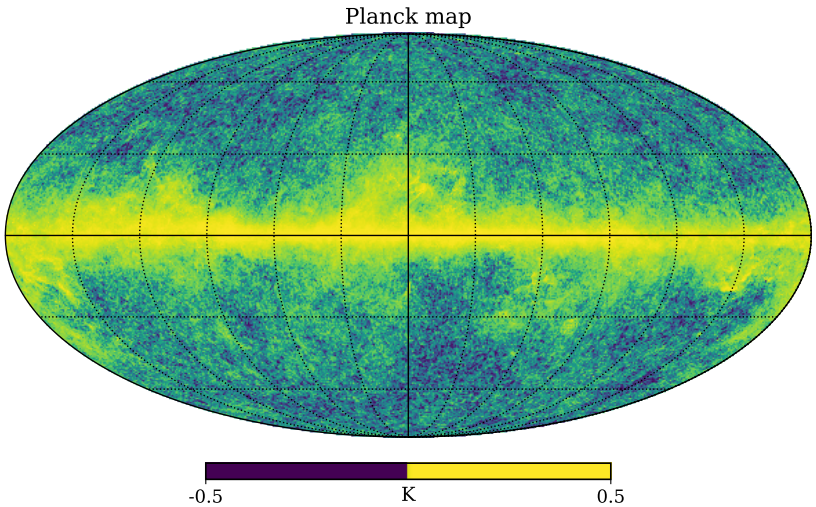

Figure: A full-sky intensity map, HFI 217 GHz, of the public Planck Release 3 data.

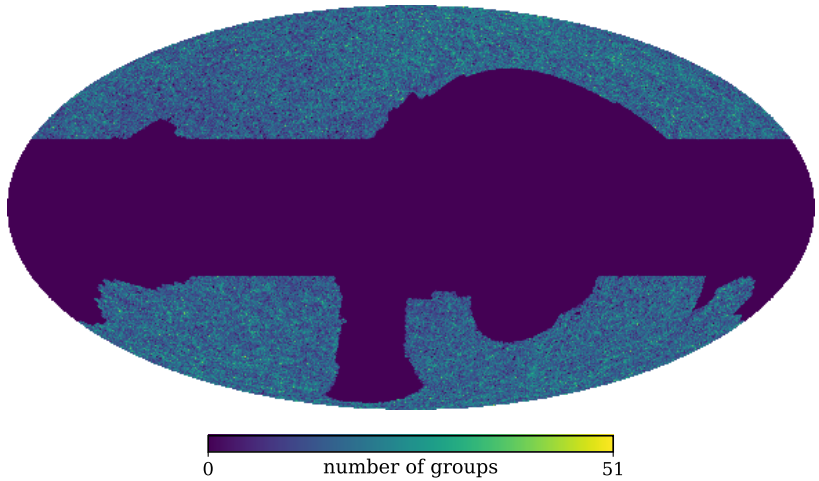

Figure: **Baseline sample**: $\sim 5.7 \times 10^6$ clusters with $M > 10^{13.0}\mathrm{M}_\odot/\mathrm{h}$.

The Data Release 9 of DESI Legacy Imaging survey (Yang et al., 2021) (Yang et al., 2022)

Baseline sample: $\sim 5.7 \times 10^6$ clusters with $M > 10^{13.0}\mathrm{M}_\odot/\mathrm{h}$.

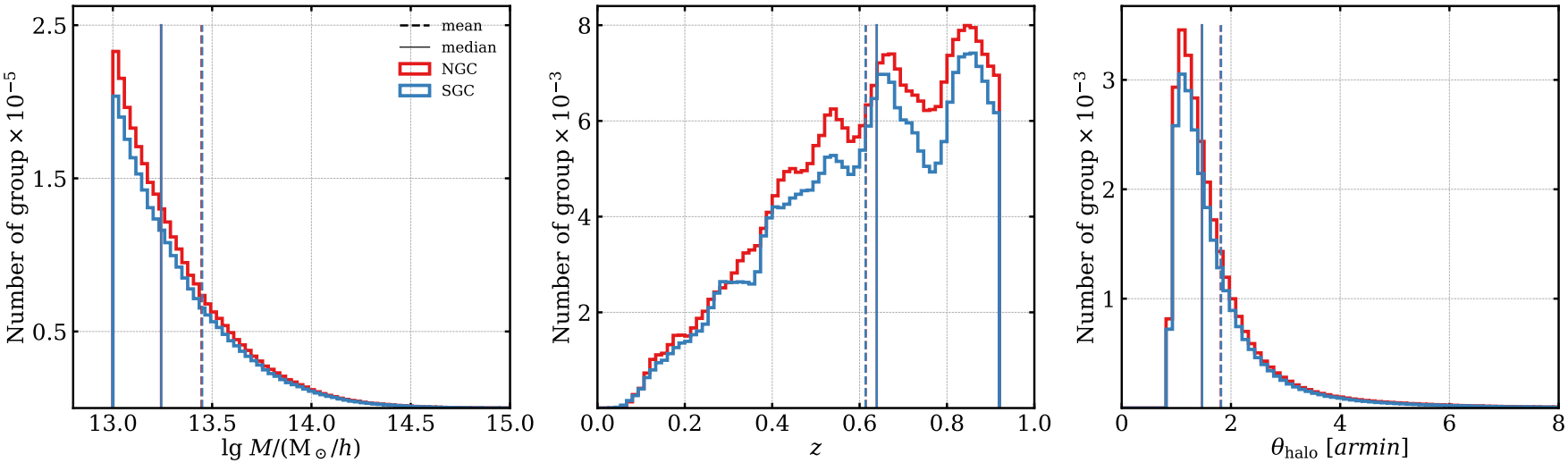

Figure: The mass, redshift and angular radius distributions of the clusters.

Methodology

ΔT_{kSZ} (AP filter) (Chen et al., 2022)

To suppress the large scale-noise, such as primary CMB fluctuation, we apply aperture (AP) filter on the Planck CMB map.

$$W_{\rm AP}(\theta) = \frac{1}{\pi\theta_{\rm AP}^2} \begin{cases} 1, & \theta \leq \theta_{\rm AP} \\ -1, & \theta_{\rm AP} < \theta \leq \sqrt{2}\theta_{\rm AP} \\ 0, & \theta > \sqrt{2}\theta_{\rm AP} \end{cases} \tag{2}$$

$$\Delta T_{\rm kSZ}^{\rm AP}(\boldsymbol{\theta}) = \int d^2\theta' W_{\rm AP}(\boldsymbol{\theta} - \boldsymbol{\theta}') T_{\rm map}(\boldsymbol{\theta}') \,, \tag{3}$$

Actually, we apply the AP filter in the spherical harmonic space:

$$W_{\rm AP}(\ell) = \frac{2}{\ell\theta_{\rm AP}} [2J_1(\ell\theta_{\rm AP}) - \sqrt{2}J_1(\sqrt{2}\ell\theta_{\rm AP})]. \tag{4}$$

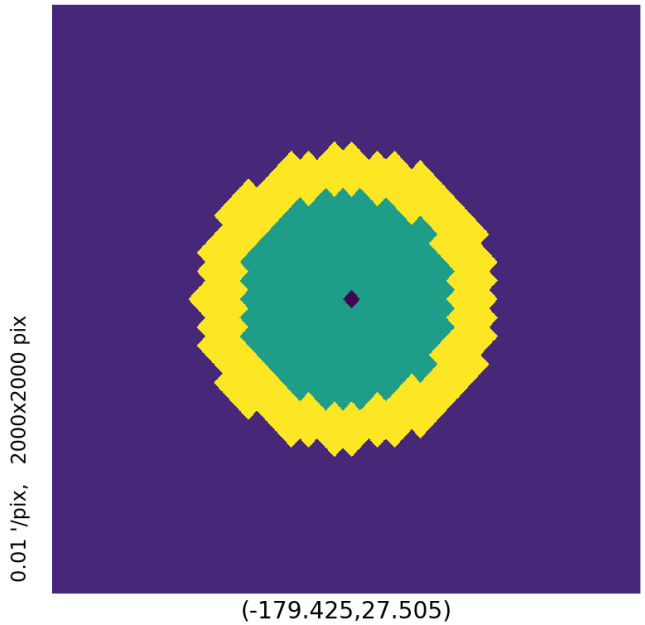

Figure: AP filter, $\theta_{\rm AP} = 3'$

Pairwise kSZ

The kSZ temperature:

$$\delta T_{kSZ}(\hat{\boldsymbol{n}}) = -\bar{\tau} T_{CMB} \boldsymbol{v}_e(\boldsymbol{x}) \cdot \hat{\boldsymbol{n}} \tag{5}$$

The pairwise kSZ:

$$T_{\mathrm{pkSZ}}(\boldsymbol{r}) \equiv \left\langle \delta T_{i,\mathrm{kSZ}}(\boldsymbol{x}+\boldsymbol{r}) - \delta T_{j,\mathrm{kSZ}}(\boldsymbol{x}) \right\rangle_{\boldsymbol{x}} \neq 0\,. \tag{6}$$

By symmetry,

$$T_{\mathrm{pkSZ}}(\boldsymbol{r}) = T_{\mathrm{pkSZ}}(r)\cos\theta\,, \tag{7}$$

where $T_{\mathrm{pkSZ}}(r)$ is the pair kSZ when $\boldsymbol{r}$ is parallel to the line of sight.

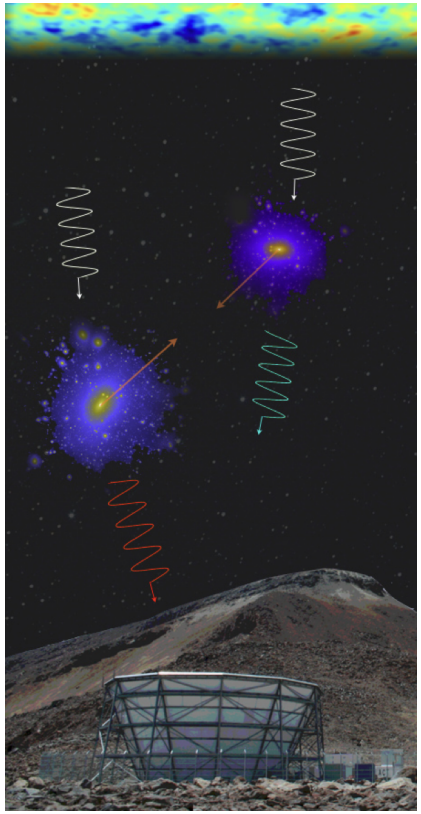

Estimator of the pairwise kSZ power spectrum multipoles

The pairwise kSZ power spectrum multipoles:

$$\hat{P}^{\ell}_{\rm kSZ}(\boldsymbol{k}) = -\frac{2\ell+1}{A}\int d^3s_1 \int d^3s_2 e^{-i\boldsymbol{k}\cdot\boldsymbol{s}_{12}}\mathcal{L}_{\ell}(\hat{\boldsymbol{k}}\cdot\hat{\boldsymbol{n}}_{12})[\delta T(\boldsymbol{s}_1)\delta n(\boldsymbol{s}_2) - \delta n(\boldsymbol{s}_1)\delta T(\boldsymbol{s}_2)]\,, \tag{8}$$

Furthermore, we average the measured $\hat{P}^{\ell}_{\rm kSZ}$ within each k bin:

$$\hat{P}^{\ell}_{\rm kSZ}(k) = \int \frac{d\Omega_k}{4\pi}\hat{P}^{\ell}_{\rm kSZ}(\boldsymbol{k}) = \frac{1}{N_{\rm mode}}\sum_{k_i\le k<k_{i+1}}\hat{P}^{\ell}_{\rm kSZ}(\boldsymbol{k}) \tag{9}$$

Theory model

The linear density-weighted pairwise kSZ power spectrum:

$$P_{\rm kSZ}(k,\mu) = \left(\frac{T_{\rm CMB}\bar{\tau}}{c}\right) 2iaHf\mu(b+f\mu^2)\frac{P_{\rm m}(k)}{k}\exp[-k^2\mu^2\sigma_z^2/H^2]\,. \qquad (10)$$

We expand P_{kSZ} in Legendre polynomials $\mathcal{L}_\ell$:

$$P^\ell_{\rm kSZ}(k) = \frac{2\ell+1}{2}\int_{-1}^{1} d\mu \mathcal{L}_\ell(\mu) P_{\rm kSZ}(k,\mu)\,. \qquad (11)$$

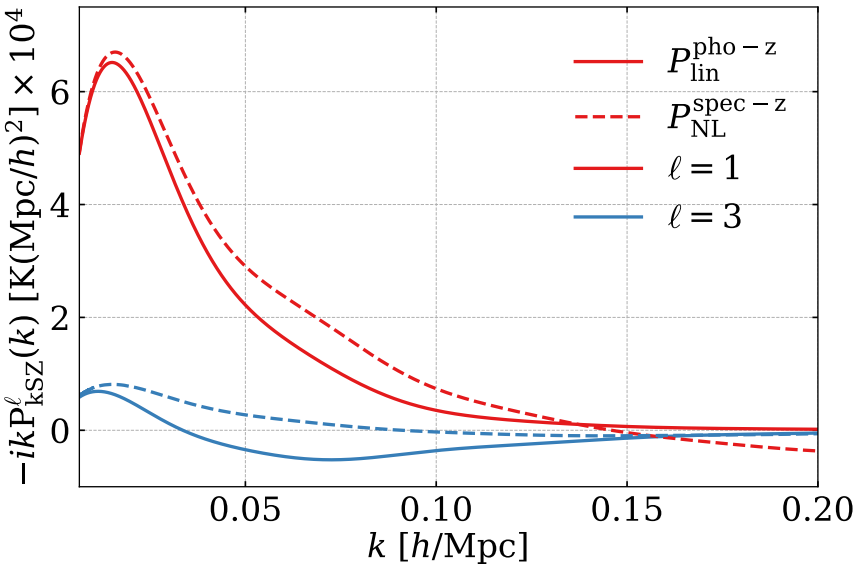

Figure: Theoretical predictions of the pairwise kSZ multipoles.

Survey window functions (Wilson et al., 2017; Beutler et al., 2017)

Dipole including window function effect:

$$\tilde{P}^{\ell=1}_{\rm kSZ}(k) = -i4\pi \int ds\, s^2 j_{\ell=1}(ks)\xi^{\ell=1}_{\rm kSZ}(s)\left(Q_0(s) + \frac{2}{5}Q_2(s)\right), \qquad (12)$$

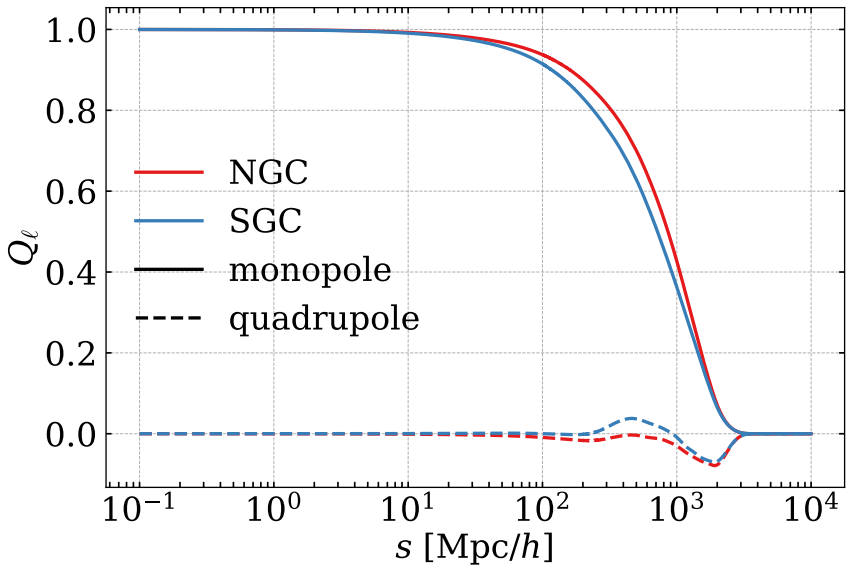

Figure: Multipoles of survey window function for the baseline sample, which are used to compute the masked pairwise kSZ power dipole.

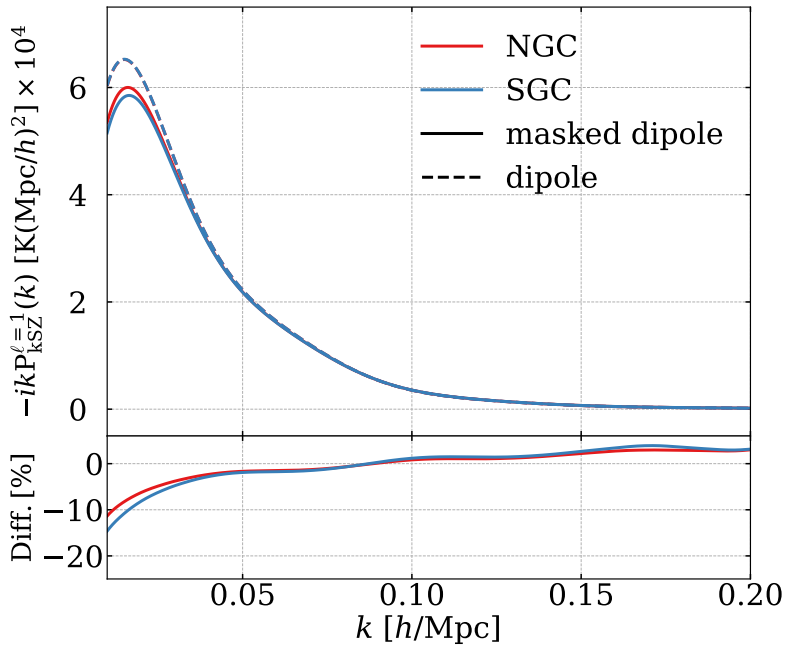

Figure: Theoretical predictions of the pairwise kSZ dipole.

Results

Pairwise kSZ dipole

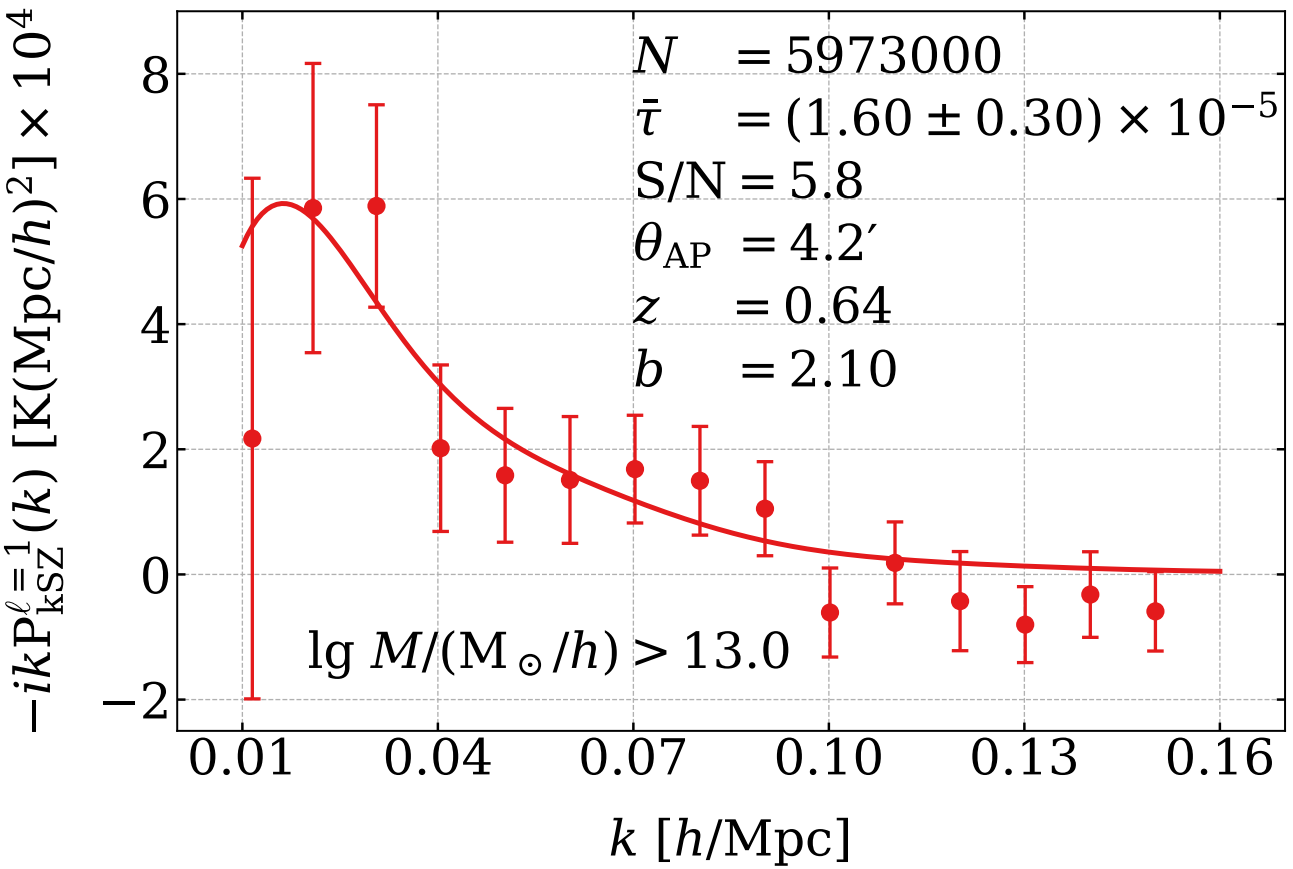

Figure: The pairwise kSZ dipole measurements of the baseline samples compared with the theoretical template (solid line).

$\bar{\tau}$ and $\mathrm{S/Ns}$

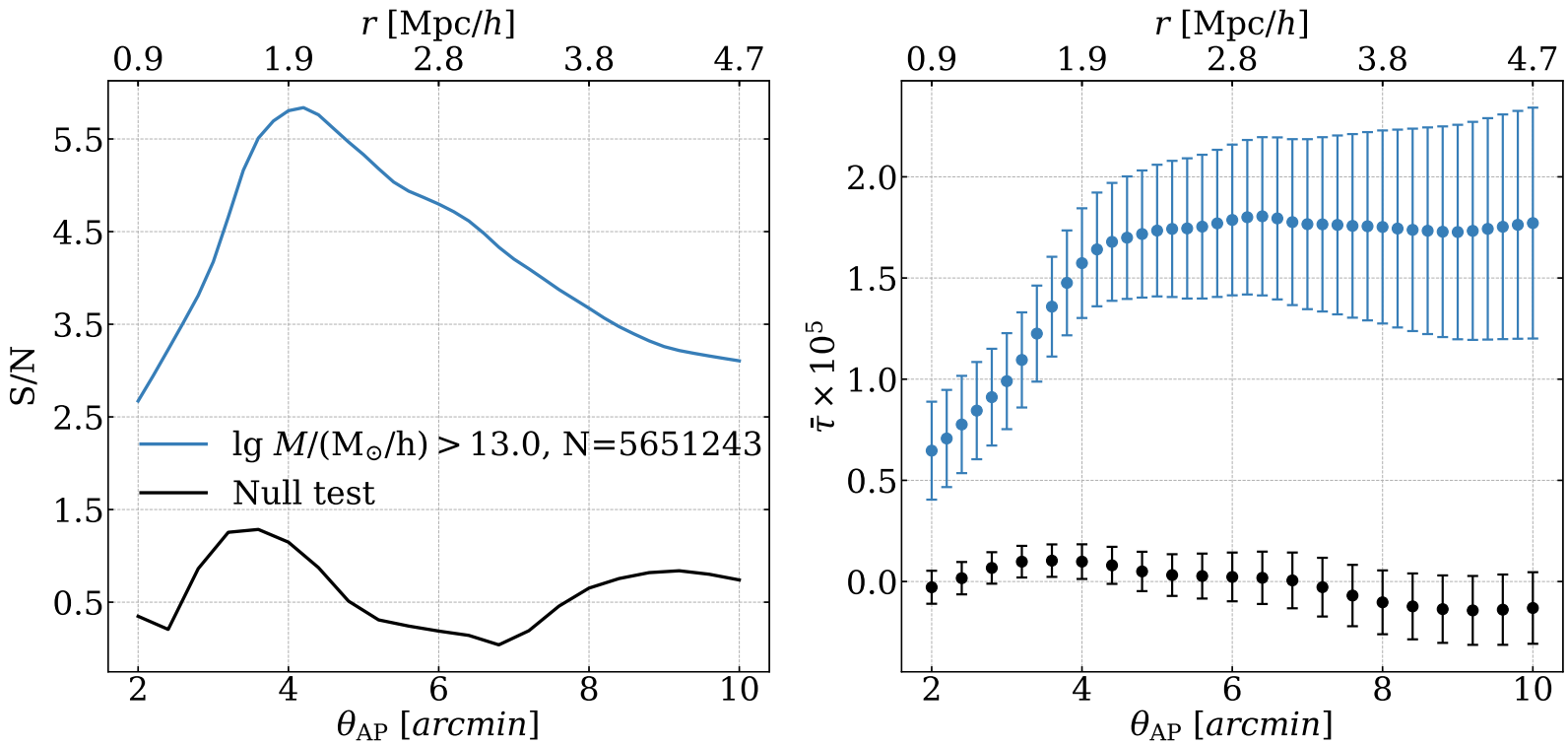

Figure: Left: The detection $\mathrm{S/N}$ profiles (blue line) of the baseline sample by adopting different AP filter radii (θ_{AP}), and the black line is the null test. Right: The corresponding measured $\bar{\tau}$ profiles.

$f_{\rm gas}$ and $\sigma_{\rm R}$

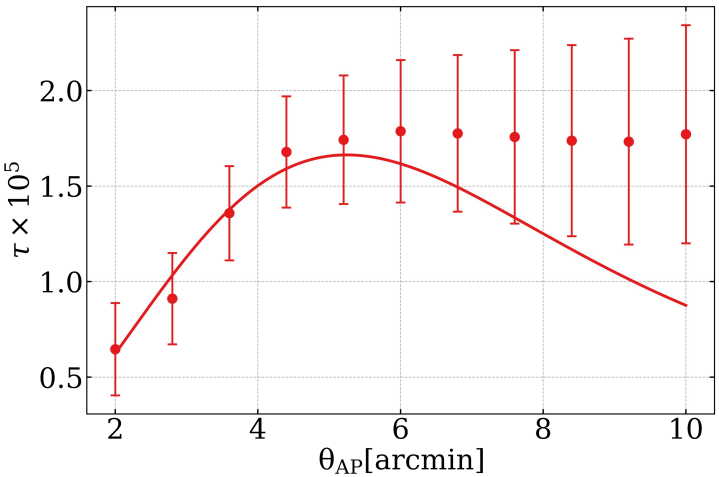

$$N(\theta) = \frac{1}{2\pi\sigma_R^2} e^{-\theta^2/(2\sigma_R^2)}$$

$$\tau(\theta_{\rm AP}) = \frac{\sigma_{\rm T} f_{\rm gas} M_{med}}{\mu_e m_p D_{\rm A}^2(z_{med})} \int \frac{d^2\ell}{(2\pi)^2} W(\ell\theta_{\rm AP}) N(\ell) B(\ell)$$

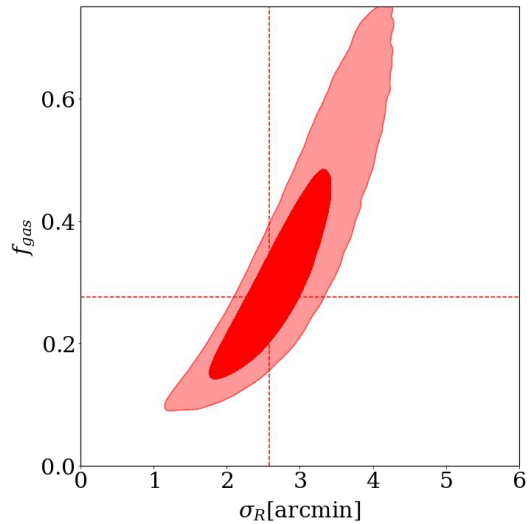

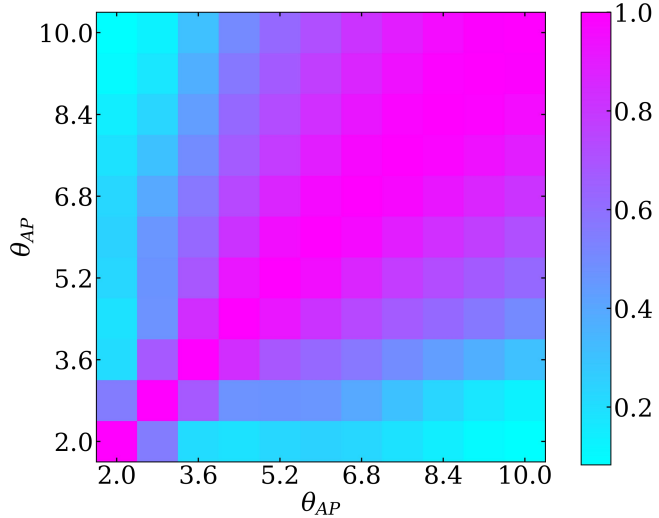

Figure: Constraint on $f_{\rm gas}$ and $\sigma_{\rm R}$ for the baseline sample.

Other samples: different masses

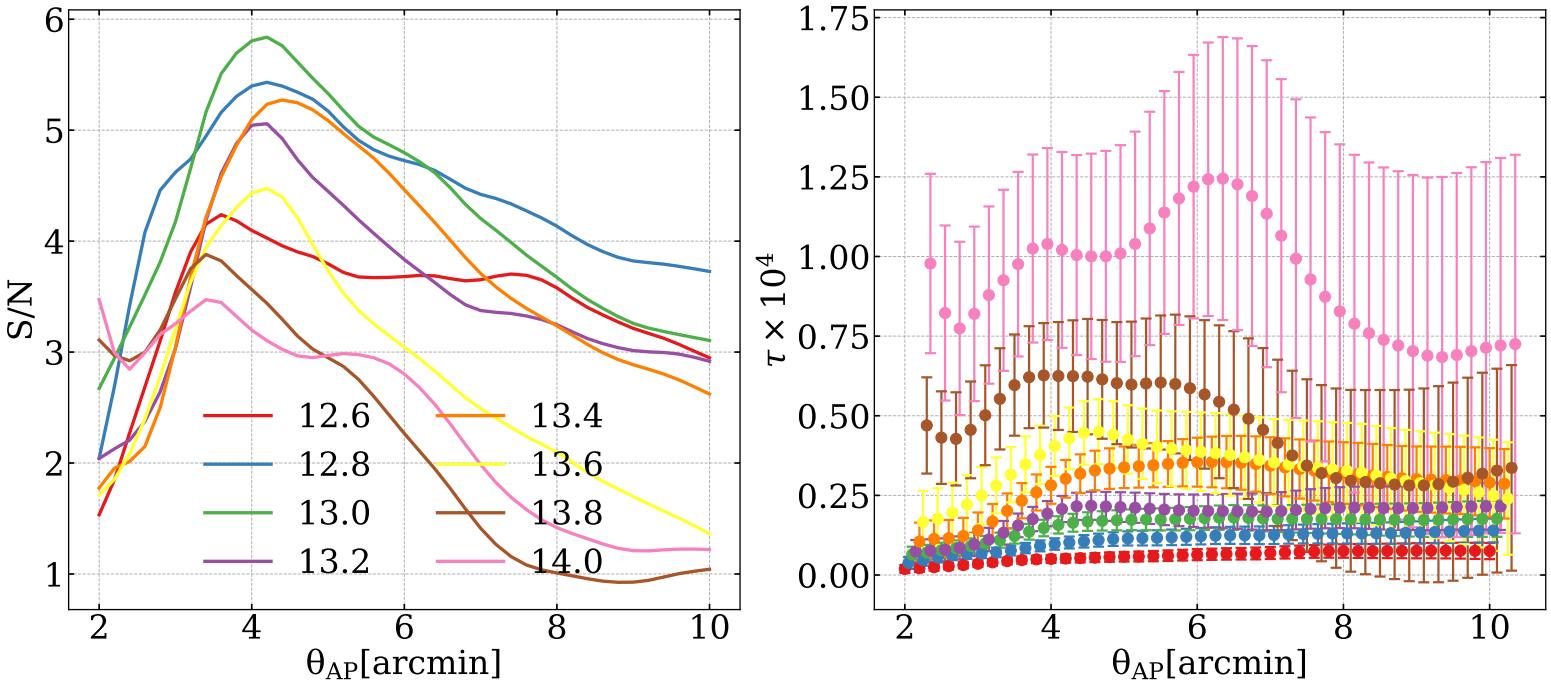

Figure: The results of cluster samples with different mass threshold values.

$\bar{\tau} - M$ relationship

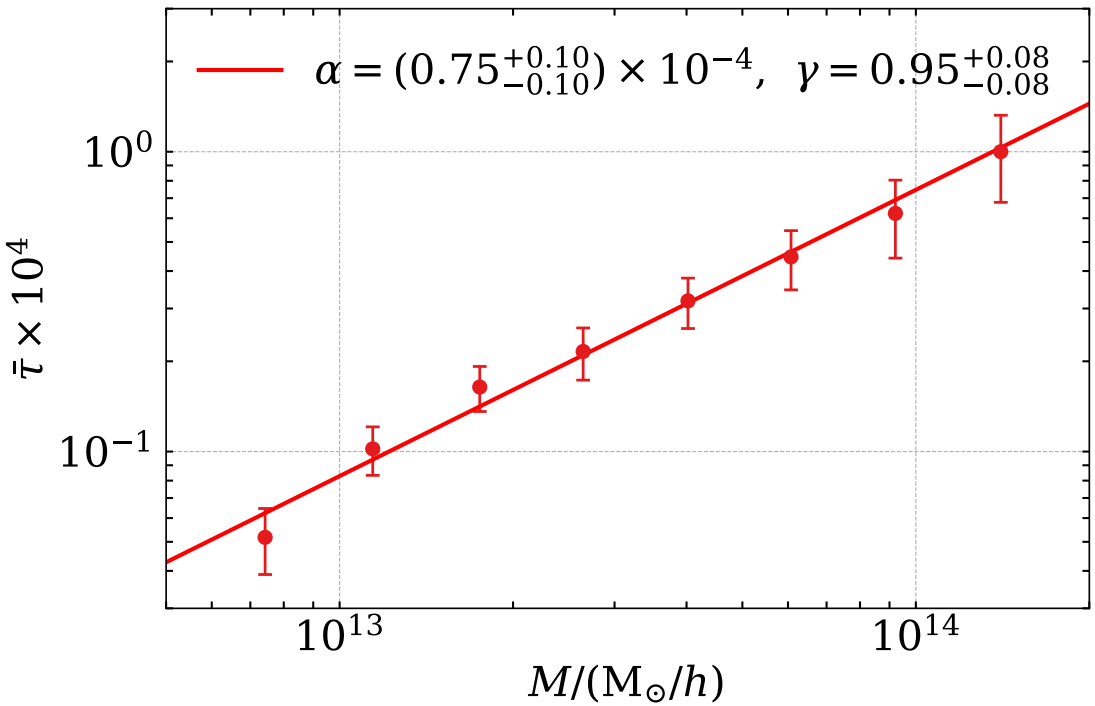

Figure: $\bar{\tau} - M$ relationship with $\theta_{\mathrm{AP}} = 4.2\ \mathrm{armin}$. Fitting model: $\log \bar{\tau} = \gamma(\log\ M - 14) + \log \alpha$.

Other samples: different redshifts

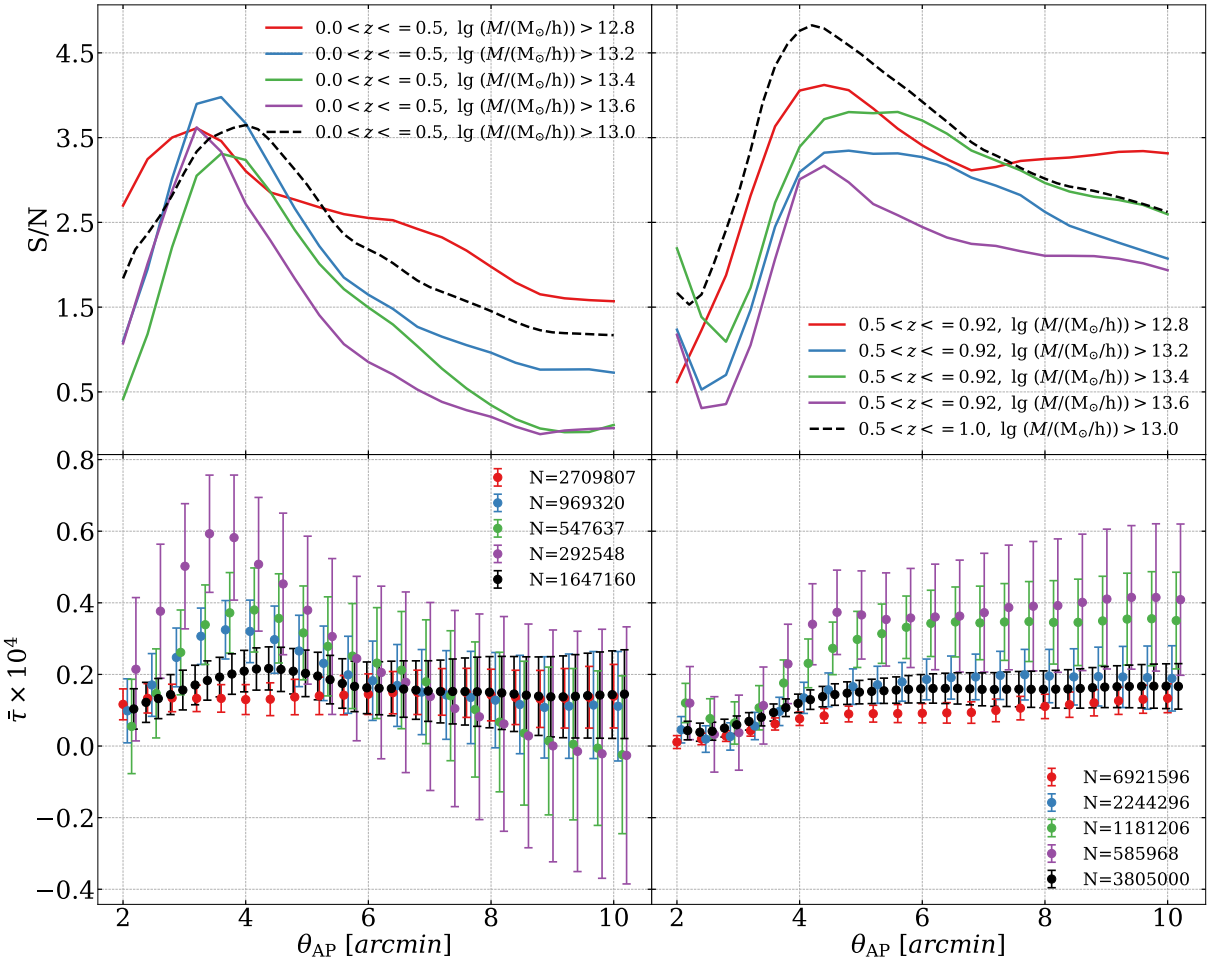

Figure: The samples shown on the previous page are further divided into two redshift bins.

Thanks!

F. Beutler, H.-J. Seo, S. Saito, C.-H. Chuang, A. J. Cuesta, D. J. Eisenstein, H. Gil-Marín, J. N. Grieb, N. Hand, F.-S. Kitaura, C. Modi, R. C. Nichol, M. D. Olmstead, W. J. Percival, F. Prada, A. G. Sánchez, S. Rodriguez-Torres, A. J. Ross, N. P. Ross, D. P. Schneider, J. Tinker, R. Tojeiro, and M. Vargas-Magaña. The clustering of galaxies in the completed SDSS-III Baryon Oscillation Spectroscopic Survey: anisotropic galaxy clustering in Fourier space. , 466(2):2242–2260, Apr. 2017. doi: 10.1093/mnras/stw3298.

Z. Chen, P. Zhang, X. Yang, and Y. Zheng. Detection of pairwise kSZ effect with DESI galaxy clusters and Planck. , 510(4):5916–5928, Mar. 2022. doi: 10.1093/mnras/stab3604.

N. S. Sugiyama, T. Okumura, and D. N. Spergel. A direct measure of free electron gas via the kinematic Sunyaev-Zel'dovich effect in Fourier-space analysis. , 475(3): 3764–3785, Apr 2018. doi: 10.1093/mnras/stx3362.

R. A. Sunyaev and Y. B. Zeldovich. The velocity of clusters of galaxies relative to the microwave background - The possibility of its measurement. , 190:413–420, Feb. 1980. doi: 10.1093/mnras/190.3.413.

M. J. Wilson, J. A. Peacock, A. N. Taylor, and S. de la Torre. Rapid modelling of the redshift-space power spectrum multipoles for a masked density field. , 464(3): 3121–3130, Jan. 2017. doi: 10.1093/mnras/stw2576.

X. Yang, H. Xu, M. He, Y. Gu, A. Katsianis, J. Meng, F. Shi, H. Zou, Y. Zhang, C. Liu, Z. Wang, F. Dong, Y. Lu, Q. Li, Y. Chen, H. Wang, H. Mo, J. Fu, H. Guo, A. Leauthaud, Y. Luo, J. Zhang, and Y. Zu. An Extended Halo-based Group/Cluster Finder: Application to the DESI Legacy Imaging Surveys DR8. , 909(2):143, Mar. 2021. doi: 10.3847/1538-4357/abddb2.

X. Yang, H. Xu, M. He, Y. Gu, A. Katsianis, J. Meng, F. Shi, H. Zou, Y. Zhang, C. Liu, Z. Wang, F. Dong, Y. Lu, Q. Li, Y. Chen, H. Wang, H. Mo, J. Fu, H. Guo, A. Leauthaud, Y. Luo, J. Zhang, and Y. Zu. Erratum: "An Extended Halo-based Group/Cluster Finder: Application to the DESI Legacy Imaging Surveys DR8" (2021, ApJ, 909, 143). , 930(1):98, May 2022. doi: 10.3847/1538-4357/ac66e5.

Appendix: Survey window functions (Wilson et al., 2017; Beutler et al., 2017)

The masked kSZ power spectrum including the window function is described by (Sugiyama et al., 2018):

$$\tilde{P}^{\ell}_{\rm kSZ}(k) = 4\pi(-i)^{\ell}(2\ell+1)\int ds\, s^2 j_{\ell}(ks)\sum_{\ell_1\ell_2}\begin{pmatrix} \ell & \ell_1 & \ell_2 \\ 0 & 0 & 0 \end{pmatrix}^2 \xi^{\ell_1}_{\rm kSZ}(s)Q_{\ell_2}(s), \quad (13)$$

and the window function multipoles characterizing the distortion of the survey geometry are gived by

$$Q_{\ell}(s) \propto \sum_{\boldsymbol{s}_1}\sum_{\boldsymbol{s}_2}\frac{1}{s^3}RR(s, \hat{\boldsymbol{n}}_{12}\cdot\hat{\boldsymbol{s}})\mathcal{L}_{\ell}(\hat{\boldsymbol{n}}_{12}\cdot\hat{\boldsymbol{s}})\delta_D(s-|\boldsymbol{s}_{12}|), \quad (14)$$

For the dipole, the expansion of eq. (13) can be linearly truncated as

$$\tilde{P}^{\ell=1}_{\rm kSZ}(k) = -i4\pi\int ds\, s^2 j_{\ell=1}(ks)\xi^{\ell=1}_{\rm kSZ}(s)\left(Q_0(s)+\frac{2}{5}Q_2(s)\right), \quad (15)$$

Survey window functions (Wilson et al., 2017; Beutler et al., 2017)

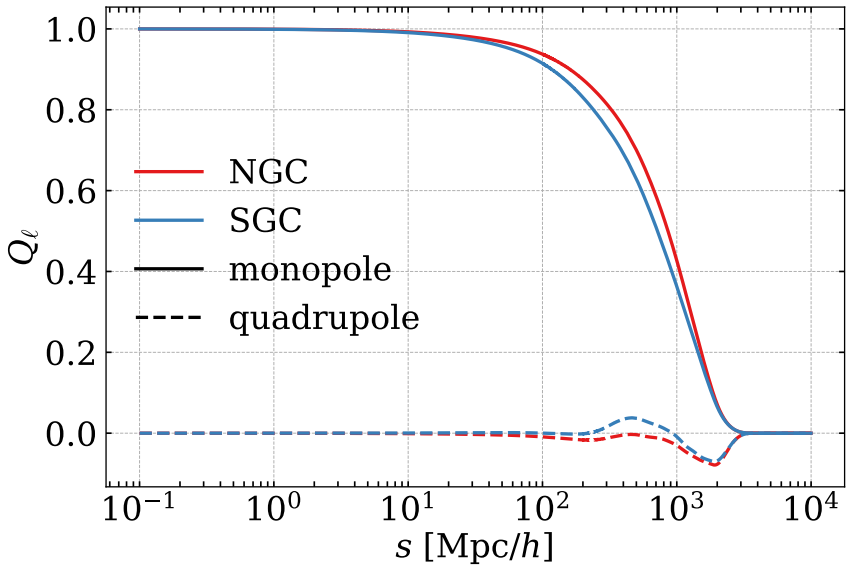

Figure: Multipoles of survey window function for the baseline sample, which are used to compute the masked pairwise kSZ power dipole.

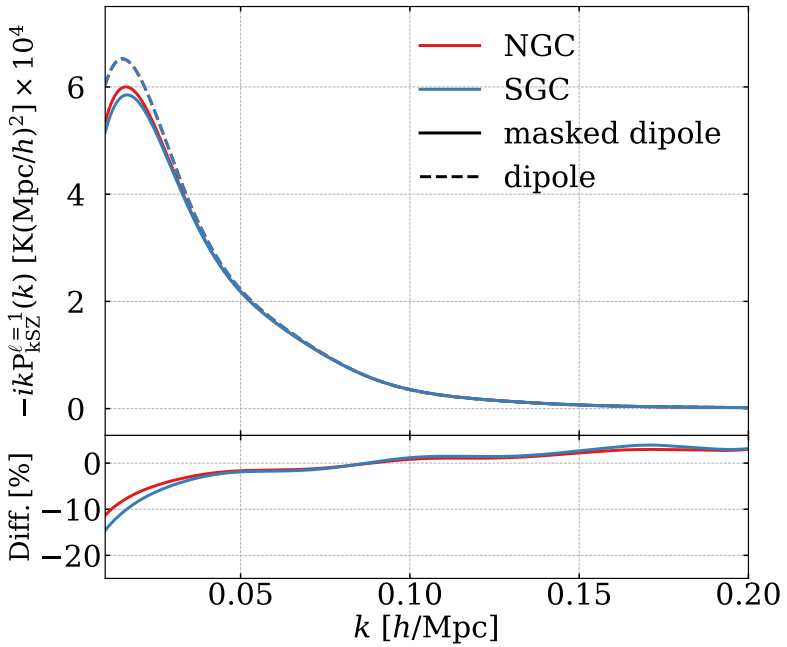

Figure: Theoretical predictions of the pairwise kSZ dipole.

Nonlinear model

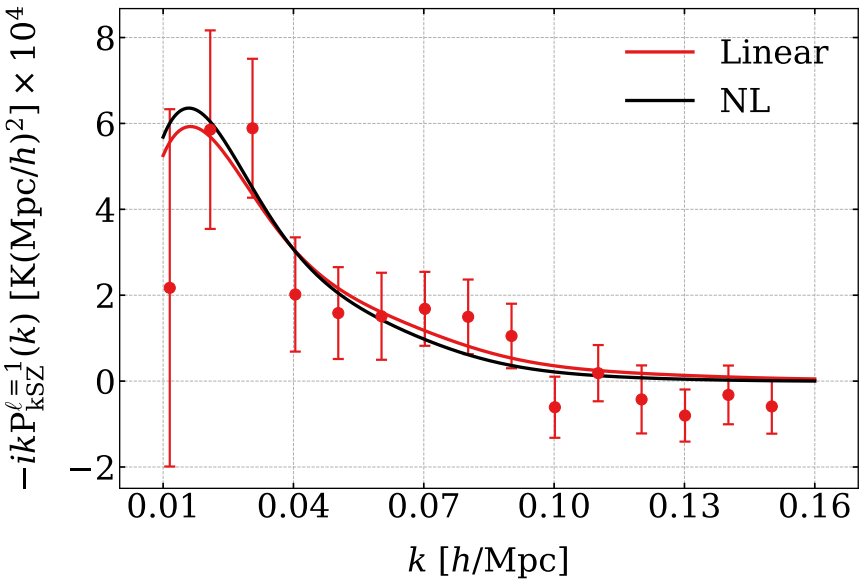

Figure: Nonlinear model.

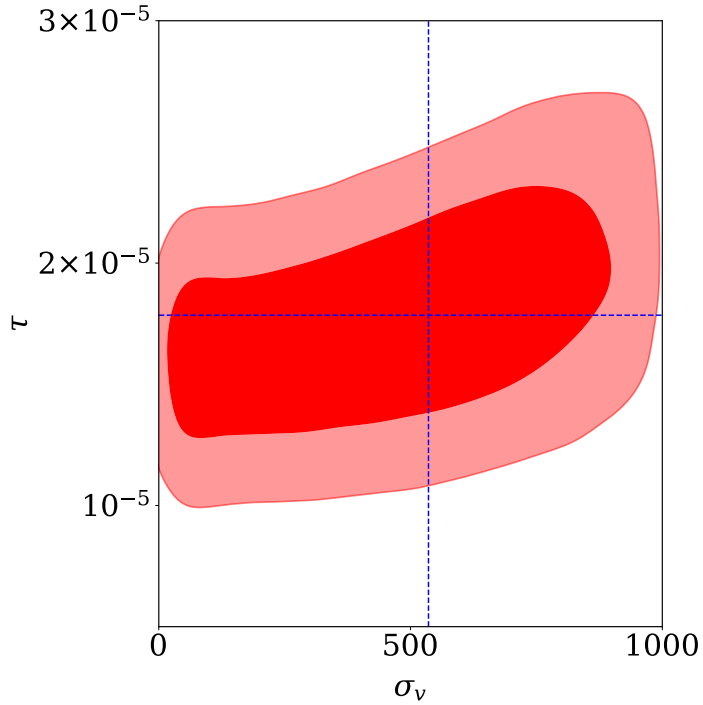

Figure: Run mcmc.

Theory model

The pairwise kSZ power spectrum:

$$P_{\rm kSZ}(\boldsymbol{k}) = \left\langle -\frac{V}{N^2}\sum_{i,j}\left[\Delta T_{i,\rm kSZ} - \Delta T_{j,\rm kSZ}\right] e^{-i\boldsymbol{k}\cdot\boldsymbol{s}_{ij}} \right\rangle . \tag{16}$$

The LOS pairwise velocity power spectrum:

$$P_{\rm pv}(\boldsymbol{k}) = \left\langle -\frac{V}{N^2}\sum_{i,j}\left[\boldsymbol{v}_i\cdot\hat{\boldsymbol{n}}_i - \boldsymbol{v}_j\cdot\hat{\boldsymbol{n}}_j\right] e^{-i\boldsymbol{k}\cdot\boldsymbol{s}_{ij}} \right\rangle . \tag{17}$$

We get

$$P_{\rm kSZ}(\boldsymbol{k}) \simeq \frac{T_{\rm CMB}\bar{\tau}}{c} P_{\rm pv}(\boldsymbol{k}) , \tag{18}$$

Theoretically,

$$P_{\rm pv}(\boldsymbol{k}) = \left(i\frac{aHf}{\boldsymbol{k}\cdot\hat{\boldsymbol{n}}}\right)\frac{\partial}{\partial f}P_{\rm s}(\boldsymbol{k}) , \tag{19}$$

where $P_{\rm s}(\boldsymbol{k})$ is the galaxy power spectrum.
The galaxy power spectrum for photo-z:

$$P_{\rm s} = (b + f\mu^2)^2 P_{\rm m}(k)\exp[-k^2\mu^2\sigma_z^2/H^2] . \tag{20}$$

Covariance Matrix (The jackknife (JK) method) (Sugiyama et al., 2018)

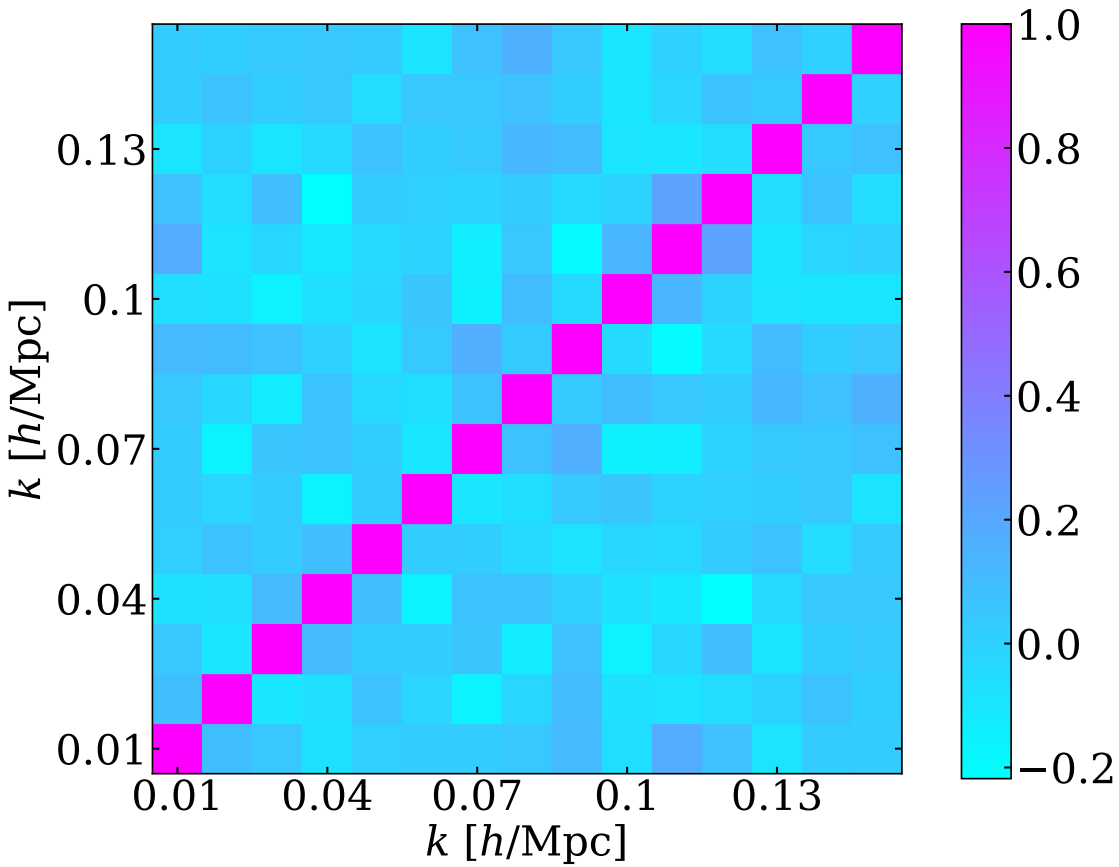

Figure: The correlation coefficient $C_{ij}/(\sqrt{C_{ii}}\sqrt{C_{jj}})$ of Baseline sample.

Past work

kSZ effect measurement - status

Current ~ 5σ

Credit: Sudeep Das

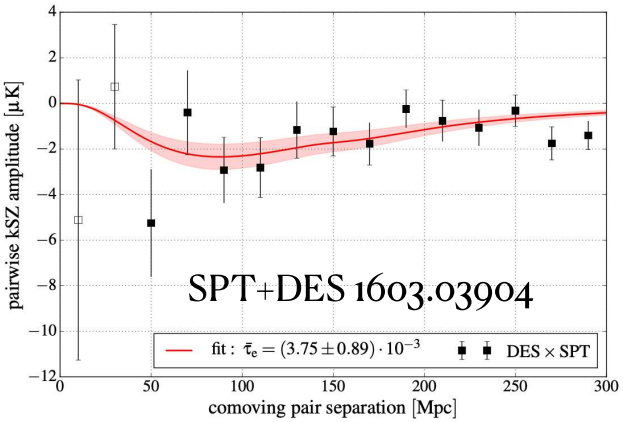

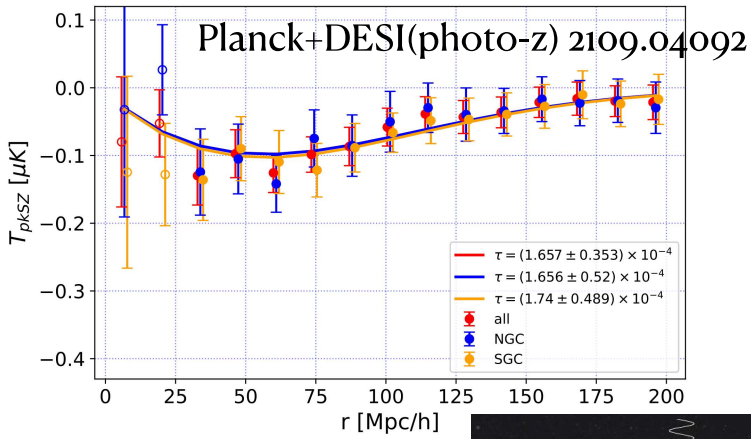

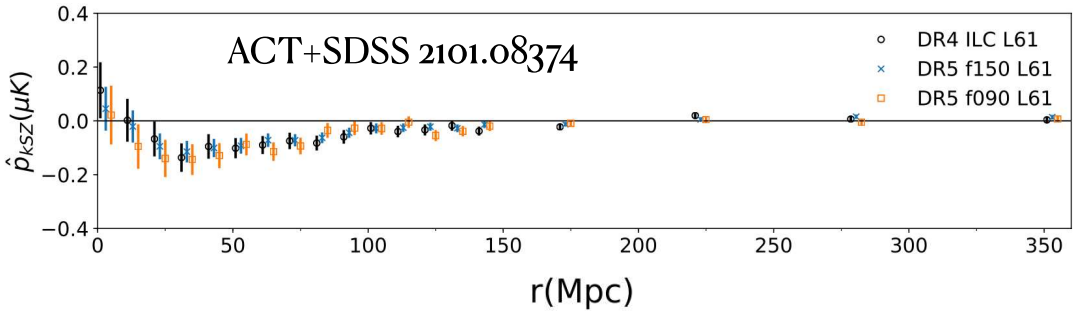

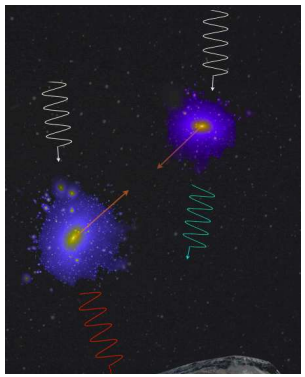

Past work

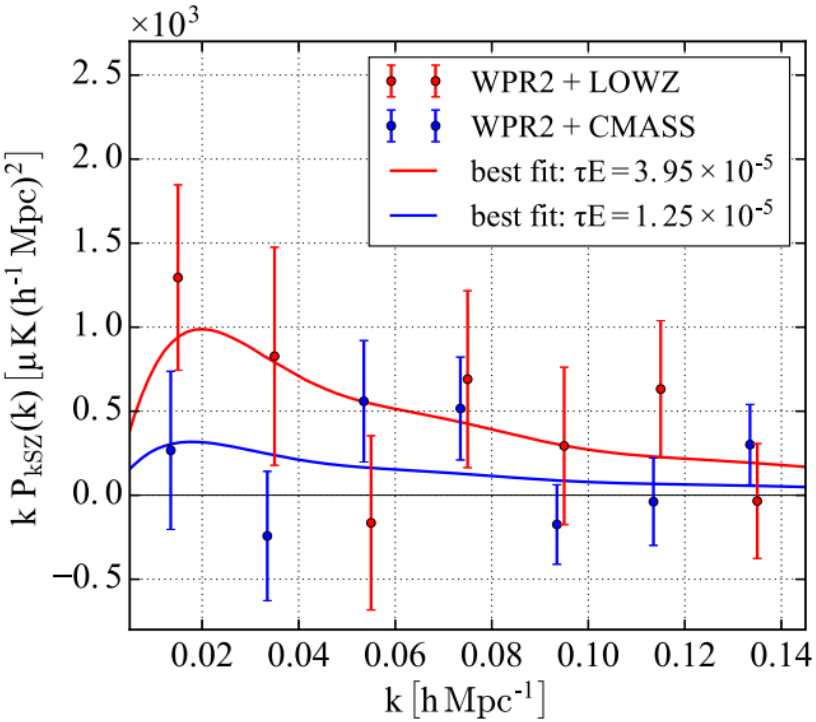

Figure 5. Pairwise kSZ power spectrum dipoles measured from the WPR2 CMB map (Section 2.1) with both the LOWZ (red symbols) and CMASS (blue symbols) samples (Section 2.2) compared with the best-fitting models (Section 3) including the window function correction (Section 5) (red and blue solid lines). The kSZ temperature per each galaxy is estimated using the AP filter with 5 arcmin (4 arcmin) aperture radius for the LOWZ (CMASS) sample. The errorbars shown are derived from the 1σ JK errors (Section 6). Using the fitting range $k = 0.015$–$0.135\,h\,\mathrm{Mpc}^{-1}$ with 7 separation bins, we find $\tau E = (3.95 \pm 1.62) \times 10^{-5}$ for LOWZ and $\tau E = (1.25 \pm 1.06) \times 10^{-5}$ for CMASS, corresponding to S/N = 2.44 and 1.18, respectively.

MNRAS **475,** 3764–3785 (2018)